Structural Health Monitoring
XX(X):1–17
©The Author(s) 2019
Reprints and permission:
sagepub.co.uk/journalsPermissions.nav
DOI: 10.1177/ToBeAssigned
www.sagepub.com/
SAGE

Analysis of Barely Visible Impact Damage Severity with Ultrasonic Guided Lamb Waves

Ifan Dafydd[1] and Zahra Sharif Khodaei[1]

Abstract

Barely visible impact damage (BVID) is one of the most common types of damage in carbon fibre reinforced polymer (CFRP) composites structures. This paper investigates the potential of using Ultrasonic Guided Waves (UGWs) to characterise the through thickness severity of BVID in thin CFRP structures. In the first step, Laser Doppler Vibrometer (LDV) was used to capture the full damage interaction of the wavefield excited by a piezoelectric actuator. Damage scattered wavefield for 4 different severities were studied to find the best parameters for characterising the severity of damage. To reduce the overall acquisition time and size of data collected using the LDV, the measured signals were reconstructed from a singular broadband chirp response using a post-processing algorithm. From the full wavefield analysis obtained at a wide range of toneburst frequencies, the results showed that BVID severity could be characterised using UGWs and that the A_0 mode, dominant at lower frequencies, gave better results than the S_0 mode. In the second step, the parameters for characterising the damage severity was applied to a spars network of transducers as an in-service SHM methodology. The damage was successfully detected and located. In addition, the transducers path close to the predicted damage location were utilised to successfully quantify the damage severity based on the proposed damage index (DI).

Keywords

Lamb waves, structural health monitoring, laser Doppler vibrometer, barely visible impact damage, ultrasonics, non-destructive inspection, damage severity

Introduction

As composite materials become more and more popular in aerospace applications, it is critical that non-destructive inspection (NDI) methods advance to deal with complex composite failure mechanisms. Unlike traditional metallic materials, they are more susceptible to barely visible impact damage (BVID) from foreign objects during their active life which can cause a drastic reduction of structural properties. A relatively new and promising approach to assessing the structure during its active life and detecting these kinds of damages is by Structural Health Monitoring (SHM).

One can define SHM as a real time damage identification method that aims to reduce maintenance costs whilst improving reliability and safety [1]. It can also broadly be split into four, increasingly difficult levels that usually relies on information from the previous level. These four levels are the detection of damage, the localisation of damage, the identification of the type and severity of damage present and lastly life prognosis of the damaged structure [2].

This work focuses on ultrasonic guided Lamb wave (UGW) based SHM which have been proven to be very effective at damage detection [1, 3]. These waves can be excited and sensed in a structure using a network of lightweight, surface mounted piezoelectric transducers [4, 5, 6] and have been utilised to detect defects in both metallic and composite structures by many researchers [7, 8, 9, 10, 11]. Mitra and Gopalakrishnan published a review paper on the developments in UGW based SHM, including the fundamental concepts of propagation as well as its application in SHM [12]. In order to detect the defects successfully, many of the UGW methods require a baseline set of measured signals obtained when the structure is known to be free of defects. Damage can then be detected as changes in the measured signals when compared to the pristine state [13]. A list of the most common damage indices (DI) based on the differences in these signals is given by Torkamani et al. [14].

A popular way of localising a defect in a structure from changes in the recorded signals is through the use of imaging algorithms. He and Yuan presented a reverse-time migration technique to image damage by cross-correlating forward and backward propagating wavefields in composite structures using the time reversal method [11]. Huang et al. developed an improved time reversal method by employing a weight vector that composed of a window function and amplitude dispersion to improve damage localisation using an imaging algorithm [15]. Zhao et al. developed a reconstruction algorithm for probabilistic inspection of defects (RAPID) method which is based on a novel correlation technique using the baseline and current signals [16]. Liu et al. combined the time reversal technique with a modifed RAPID algorithm to detect delamination in composite plates [17].

[1] Department Of Aeronautics, Imperial College London, U.K.

Corresponding author:
Ifan Dafydd, Department Of Aeronautics, Imperial College London, South Kensington Campus, London, SW7 2AZ, UK.
Email: i.dafydd15@imperial.ac.uk

The method used in this work is based on the delay & sum method, developed and utilised by Michaels et al. [18] and Sharif-Khodaei et al. [19]. This uses the time of flight principle and a baseline set of comparison signals to localise damage to draw a locus of potential damage location on a structure. Salmanpour et al. proposed a temperature compensation method to improve the delay & sum method over a range of different temperatures [20]. Lu et al. developed a method of increasing the DI obtained using the delay & sum method by drawing both ellipses and hyperbolas on actuator-sensor pair signals [21]. Zeng et al. proposed a damage imaging method based on the delay & sum method that takes into account multipath scattering from boundary conditions in the structure to improve damage localisation [22].

However, whilst these methods, and many more, have been able to detect and locate damage, being able to identify its type and severity from the signals obtained with a sparse network of transducers still remains a challenge. Ihn and Chang published two sequential papers in which a proposed diagnostic technique was applied to monitor hidden fatigue crack growth in riveted fuselage joints and a cracked metallic plate repaired with a bonded composite patch [23, 24]. Memmolo et al. utilised a wave reflection method based on Snell's law to detect, locate and outline the extent of severity of a stringer-skin disbond [25] whilst Pillarisetti and Talreja quantified damage severity from the PST of signals but these were cracks in the structure, not delamination and their algorithm did not localise the damage [26].

The limiting factor with using a sparse network of transducers is that the UGW data obtained at each transducer is one dimensional, $U_{PZT}(t)$, and so gives very limited information on the UGW interaction with damage through the structure. To get full wavefield information across the structure, $U(x, y, t)$, a laser Doppler vibrometer (LDV) can be used to sense the UGW in both the spatial and temporal domain. A group led by Staszewski published three sequential papers on utilising a scanning laser vibrometer for SHM [27] [28] [29]. He also published a review paper of using a LDV for SHM [30].

To enhance the visualisation of a damaged area, many authors including Ruzzene et al. [31], Kudela et al. [32] and Zak et al. [33] used the root mean square (RMS) of the LDV signals. This was also done after wavenumber-frequency filtering to separate the reflected wave from the propagating wave as Ruzzene proposes with an aluminium plate [34]. Also, in the wavenumber domain, Rogge and Leckey developed a method of determining the depth of delamination in composite structures [35]. An anomalous wave propagation imaging method to detect defects in a composite wing was shown by Chia et al. [36]. Pieczonka proposed a damage identifcation method using a LDV based on mode-conversions at regions of damage in composite panels [37]. Park et al. created an algorithm to enhance standing waves formed within delaminations and disbonds in the wavenumber-frequency domain [38]. For damage severity assessment using a LDV, Yu et al. quantified the size and severity of a crack in an aluminium plate using guided wavenumber analysis methods [39].

Yu et al. also developed a global-local rapid inspection approach using the LDV based on phased array beamforming and wavenumber analysis to reduce total inspection time and detect and quantify impact induced delamination in CFRP [40]. Another method developed to reduce total inspection time was proposed by Mesnil and Ruzzene and is based on a compressed sensing technique [41]. This reconstructs guided wavefield from a set of sparse measurements by employing information on the dispersion relations of the structure under consideration. To reduce the data size and the time required to scan at multiple frequencies, Dafydd et al. proposed using a chirp excitation when using an LDV and showed the results on composite panels with artificial delamination and impact damages [42] [43].

Most of the work mentioned above utilise the LDV as a standalone NDI technique. It cannot technically be classified as a SHM method due to the the restriction on setting up the three laser heads and data acquisition system which makes it impractical as a fast and reliable in-service maintenance approach. However, Hall and Michaels proposed combining a baseline LDV obtained wavefield data with both current and baseline signals obtained using small number of permanently mounted transducers [44] to better locate damage in a structure. This successfully detected and located damage in complex structures but did not give any information on the severity of the damage.

The challenge still remains on being able to analyse and quantify the through thickness severity of a BVID with UGWs, as is currently possible with a C-scan. This work aims to employ a LDV to carry out a fundamental investigation into the interaction between guided Lamb waves and the through thickness severity of a BVID in composite structures and then apply this information to design a damage index for use with a sparse network of transducers in a pitch-catch configuration. As the time taken for one LDV scan at one input signal takes up to 12 hours and multiple scans are required to determine the optimum input signal, the use of a chirp input signal and a toneburst reconstruction method is proposed to not only reduce acquisition time but also reduce the size of the data collected.

In this paper, the section "Composite Panels" describes the manufacturing of the composite panels, the introduction of impact damage to the panels and the traditional NDI results. This is followed by the section "Experimental Setup" which shows the experimental setup for the LDV and the proposed chirp excitation method. Then, the section "LDV Results" uses the full wavefield results as well as RMS and wavenumber filtering to characterise the severity of damage present. The section "Incorporation into in-service SHM" applies the findings from the LDV data to a sparse transducer network for in service SHM. Finally, the section "Conclusions" summarises the work and the outcomes of the paper.

Composite Panels

Geometry and Manufacturing

A 16 ply quasi-isotropic thermoset composite panel of dimensions 600x600x2mm with a layup sequence of $[0/\pm 45/90]_{2s}$ was manufactured from 8552-33%-134-IM7-12K-1200mm pre-preg sheets and cured in an autoclave according the manufacturer's guidelines. Post-curing, four smaller

identical panels of dimensions 250x250x2mm were made from the large panel via waterjet cutting. A PIC255, lead zirconate titanate (PZT) piezoelectric transducer, 10mm diameter, was bonded on each of the four panels 80x80mm from the bottom left corner in order to generate the Lamb waves. An illustration of these stages can be seen in Figure 1, where the red area highlights the area of interest around the impact damage. The geometry of this area is shown in Figure 2.

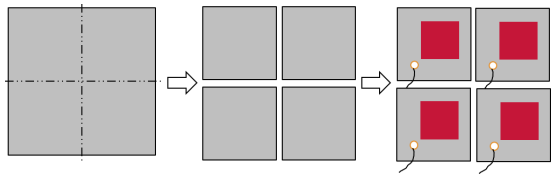

Figure 1. Schematic of the panel manufacturing stages

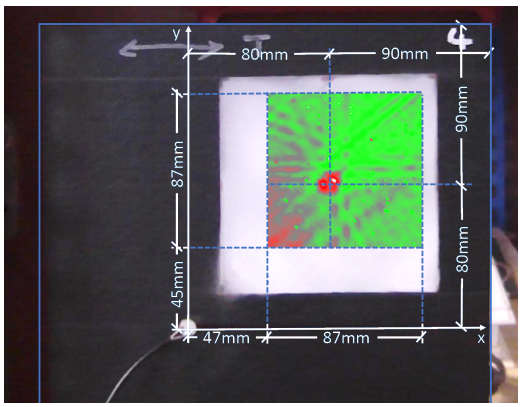

Figure 2. Highlighted area of interest around the BVID on Panel 4

Figure 3. INSTRON CEAST 9350 drop tower used to damage the panels

Impacts

Figure 3 shows the Instron Ceast 9350 drop tower machine that was used to impact the panels. A 20mm hemisphere diameter with a weight of 2.41kg was used as the impactor and the impact energies were varied by adjusting the height at which the impactor would drop from. The lowest impact energy to cause BVID was found to be 5J after carrying out an impact calibration test [45]. Panel 1 was impacted with this energy to cause the least severe damage. The higher energy impacts were then chosen at 7J, 9J and 11J respectively for panels 2, 3 and 4. The force-time history from the impacts can be seen in Figure 4 where the completely elastic 1J case was used just for calibration and caused no damage in any of the panels.

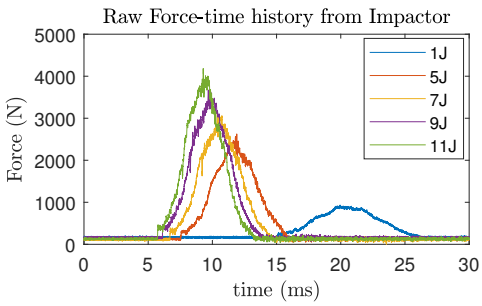

Figure 4. Impact Force data from the impactor

Traditional NDI Results

Before utilising Lamb waves to characterise the damage, the panels were tested using traditional NDI methods. This was done with an immersion ultrasonic C-scan, a hand-held ultrasonic DolphiCam and an infrared thermography (IRT) camera to verify that the impacts had caused BVID in all the panels and that their severities were increasing with higher energy levels. Ultrasonic testing is currently the most popular technique for composite laminates [46] but the setup time and scan time can be time consuming. IRT on the other hand is a much faster technique that is becoming increasingly popular [47] but its resolution is not as high as ultrasound thus both were used in this work.

The results of the immersion C-scan (top) and hand-held DolphiCam (bottom) can be seen in Figure 5 for each of the four panels. The immersion C-scan results show that both the location of the impacts and the location of the bonded PZT actuators matched for each panel whilst the hand-held DolphiCam's results focused on the exact geometry of the damage and how its through-thickness severity evolved with increasing impact energy levels. Figure 6 shows the thermography results for the four panels which were actually measured from behind, hence the horizontal symmetry in damage location. Again, the damage severity can be clearly seen with increasing impact energy. It is worth noting that the bonded PZTs visible in the thermography results are because these measurements were taken after the work in section "Incorporation into in-service SHM" was conducted.

It is also worth noting that on panel 4 a small 15mm crack was visible under good light on the rear side as shown in Figure 7. However, on the top of the panel, where the impact took place, no damage is visible and thus the damage is still a BVID from the inspection side. This shows the energy transfer through the panel during impact as is expected from laminate fracture theory.

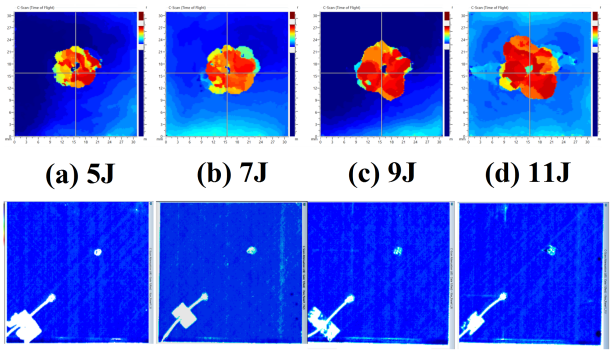

Figure 5. Ultrasonic C-scan results showing the entire panels (top) and the impacted area (bottom) from left to right 5J, 7J, 9J and 11J impact BVID

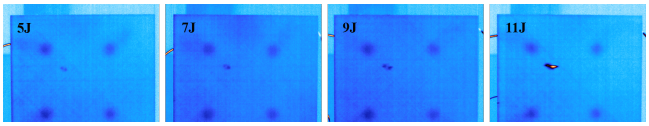

Figure 6. Thermographic imaging of panel 1, 2, 3 and 4 from left to right with increasing severity

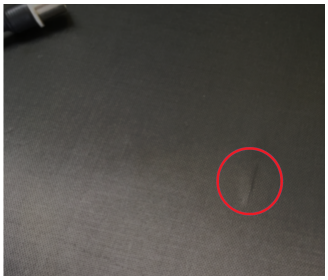

Figure 7. 15mm visible crack present on panel 4

Experimental Setup

LDV

Accurate non-contact surface velocity measurements on a structure can be obtained with an LDV which is a laser vibration measuring system based on the Doppler Shift. This allows Lamb waves and their interaction with damage to be analysed and visualised by simply defining a measurement grid of scan points with spacing small enough to fulfil the spatial (wavelength) Nyquist criterion of the ultrasonic wave modes [48]. The LDV used for this experiment is a Polytec scanning vibrometer (PSV) system, specifically, the PSV-500-3D-M model [49].

Figure 8 shows the LDV setup for capturing the UGWs. The toneburst signal was generated using an Agilent 33120A arbitrary waveform generator at an amplitude of ±2V which was then increased by the amplifier to ±100V and sent to the piezoelectric actuator bonded to the surface of the structure. The sampling frequency was set to the hardware's maximum of 2.56MHz to avoid any temporal aliasing and 2048 samples were recorded at each point to give a 0.8ms reading. 5929 point were defined in a square scan grid of 87x87mm which was dense enough to capture the wavelengths of the propagating UGWs.

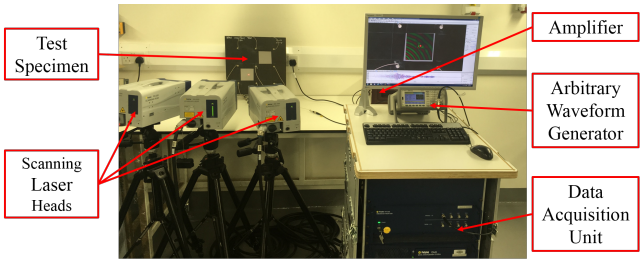

Figure 8. LDV setup for wavefield acquisition

Excitation Signal

It has been demonstrated by [50] that one of the most effective excitation signal to detect damage using Lamb waves is a narrowband Hanning windowed toneburst at a centre frequency, f_c, with a small number of cycles, n_{cycles} which can be expressed as

$$s_b(t) = w(t)\sin(2\pi f_c t)$$
$$\text{where} \quad w(t) = 0.5\left[1 - \cos\left(\frac{2\pi f_c t}{n_{cycles}}\right)\right]. \quad (1)$$

This is to minimise both dispersion of the waves and complicated boundary reflections. Figure 9 shows this signal for 5 cycles and a centre frequency of 100kHz in both the time and frequency domain. Lamb waves are multi-modal in nature and it is well documented that various types of damage interact differently with various modes [13]. This means that choosing a specific frequency where the amplitude of a particular mode is greater than the rest is important. It is also desirable to only excite the two lowest fundamental modes to simplify the signal processing. As the type of damage is unknown and the frequency which is preferred for a particular mode is also unknown, it is necessary to take measurements at a whole range of frequencies. For the panels being investigated here, 50-500kHz was the chosen range.

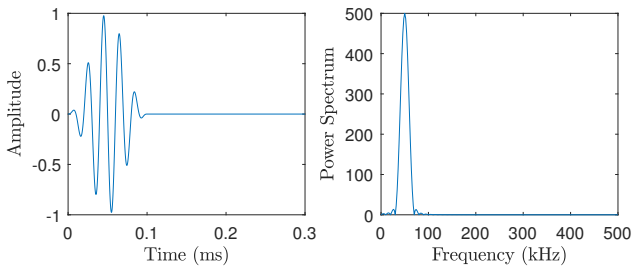

Figure 9. 5 Cycle Hanning Windowed toneburst at 50kHz centre frequency

A drawback of the LDV measurement system is the time it takes to scan an area of interest, which can be anything up to 12 hours. This is due to the number of scan points needed in the area of interest to capture the wave propagation as well as the number of averages and the time it takes the laser to move and refocus at each point. Add to this the need to scan four different panels at a whole range of narrowband, windowed tonebursts and the process becomes very time consuming. For this experiment, the chosen range was 50-500kHz in 25kHz increments and 3,5 and 10 Hanning windowed cycles

were analysed. This would require a total of 19x4x3 = 228 scans, each taking 12 hours.

To overcome this problem, a broadband linear chirp signal that covered the entire frequency range of interest was used as the input. This can be expressed as

$$s_c(t) = w(t)\sin\left(2\pi f_0 t + \frac{f_1 - f_0}{T}t^2\right)$$
$$\text{where} \quad w(t) = \begin{cases} 1, & \text{for } 0 \le t \le T \\ 0, & \text{for } t \ge T \end{cases}, \quad (2)$$

where f_0 is the starting frequency, f_1 is the final frequency and T is the time it takes to sweep from f_0 to f_1. In order to obtain adequate SNR, the duration of the chirp, T, was chosen to be 0.5ms. The starting frequency and final frequency were chosen at 50kHz and 500kHz respectively. Figure 10 shows the signal in the time domain whilst Figure 11 shows the signal in the frequency domain and its spectogram.

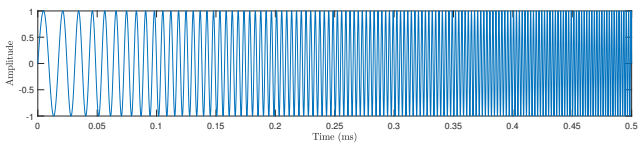

Figure 10. 50-500kHz linear chirp signal in time domain

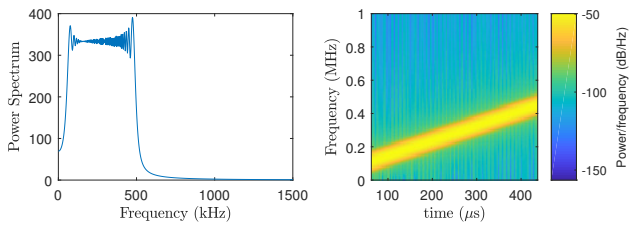

Figure 11. 50-500kHz linear chirp signal in the frequency domain (left) and its spectogram (right)

However, the signals measured using a chirp signal are very difficult to understand in the raw time domain. So, to obtain the results at a whole range of narrowband, windowed tonebursts, the data was then passed through a reconstruction algorithm given by

$$R_b(\omega) = R_c(\omega)\frac{S_b(\omega)}{S_c(\omega)} \quad (3)$$

where $R_b(\omega)$ is the toneburst response of interest, $R_c(\omega)$ is the recorded chirp response, $S_b(\omega)$ is the narrowband input toneburst of interest and $S_c(\omega)$ is the broadband chirp input signal. All the signals in Equation 3 are in the frequency domain but were measured/constructed in the time domain. A Fourier transform was therefore required to convert them to the frequency domain and then the results had to be converted back to the time domain via an inverse Fourier transform in order to visualise the Lamb waves. This method has been used in [51] to determine the best frequency and number of cycles for mode purity using an actuator and sensor in pitch-catch configuration, the delay and sum method in [52] to locate damage whilst [42] used the technique with an LDV to visualise the interaction of Lamb wave modes with delamination.

LDV Results

Introduction

As previously mentioned, Lamb waves are multi-modal in nature and generate two fundamental modes below a threshold cut-off frequency when excited with a surface mounted transducer. These are the zeroth order antisymmetric A_0 and symmetric S_0 modes. Their propagation velocities and relative amplitudes differ and are a function of the excitation frequency. The A_0 mode is more dominant at low frequencies whereas the S_0 mode is more dominant at high frequencies (in the 50-500kHz range for these panels).

As mentioned, the responses for each frequency from 50kHz to 500kHz in 25kHz increments and 3, 5 and 10 Hanning windowed cycles were extracted from the chirp signal excitation in each of the 4 panels. This meant that instead of 228 separate scans, only 4 scans were required and provided a saving of 224 x 12 hours = 2688 hours in acquisition time. After analysing the X, Y and Z displacement components of the waves separately at all of these reconstructed frequencies and number of cycles, a few instant conclusions were made. The Z-displacement showed the best SNR, 5 cycles gave the best trade off in minimising reflections but keeping a centre frequency and to isolate the A_0 mode, the frequency should be kept below 75kHz whilst to isolate the S_0 mode, the frequency should be kept above 250kHz. For the rest of this analysis, only two different excitation signal results will be shown for each case, one to isolate the A_0 mode and one to isolate the S_0 mode.

Full Wavefield Visualisation

The simplest way to analyse the data obtained with the LDV is to look at snapshots in time of the propagating UGWs as they pass through the scanned area. This requires very little post-processing of the signals, apart from a 2D median filter to get rid of any noisy scan points, and can instantly give an indication of how the waves behave and interact within the structure.

A_0 Mode Results Figure 12 shows the full wavefield results with a 5 cycle, 75kHz centre frequency toneburst for panel 1 (top) right through to panel 4 (bottom), where the A_0 mode is the dominant mode. A clear interaction can be seen between this mode and the impact damage and a few trends with increasing severity can be seen. Firstly, by looking at the wavefield image at $125.0\mu s$, (b), there is a clear increase in phase shift and amplitude reduction on the propagating wave through the damage as the severity increases. Reflections are also more prominent as the severity increases as shown at timestep $153.9\mu s$, (c), where they are almost non existent at the least severe 5J case.

S_0 Mode Results To isolate the S_0 mode, the centre frequency was chosen at 350kHz. Figure 13 shows the full wavefield results at this frequency for the four panels. The interaction of this wave mode with impact damage is very different to the A_0 mode. At $37.1\mu s$, the size of the damage can be seen, at least for the more severe cases, as the

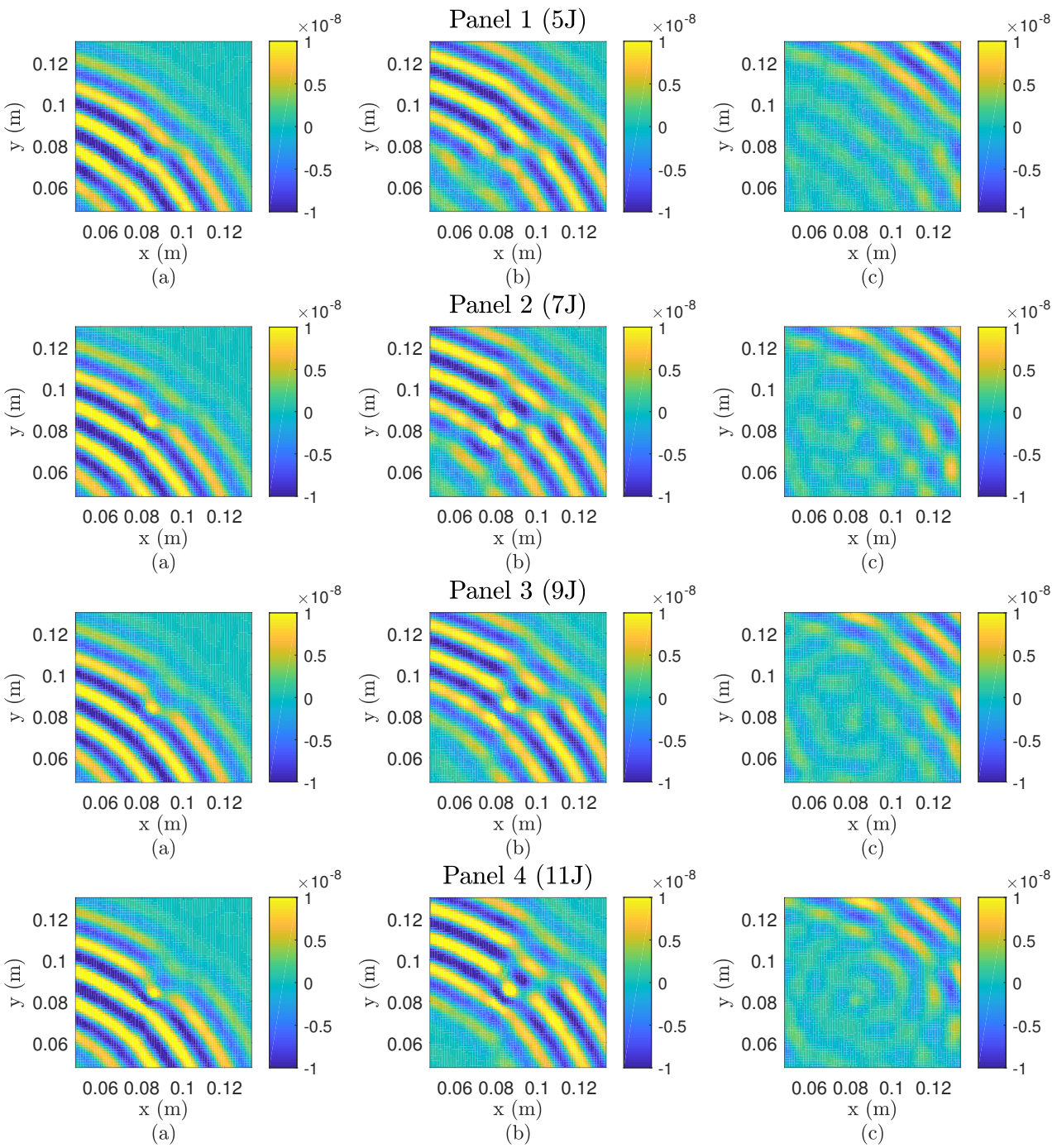

Figure 12. Impacted panels at 75kHz showing A_0 mode at (a) $110.5\mu s$, (b) $125.0\mu s$ and (c) $153.9\mu s$ respectively

propagating wave passes through. It can be observed at this timestep that the UGWs amplitude is greatly reduced in the damage region. However, in the area surrounding the BVID, the UGWs amplitude and phase are unaffected and reflections are much more difficult to see than with the A_0 mode.

By simply looking at the full wavefield, it can be concluded that the S_0 shows the geometry of the BVIDs clearly as the wave passes through it but characterising its severity and effect on the whole propagating wavefield with this data alone is difficult. On the other hand, the exact damage geometry cannot be observed by the A_0 mode but the BVIDs' severities and effect on the wavefield can be seen. The whole wavefield data shows that the more severe the BVID is, the greater the phase shifts, reflections and reduction in amplitudes of the propagating waves are.

Weighted Root Mean Square

With the discrete scan grid of spatial points, the Weighted Root Mean Square (WRMS) of the time domain signal at each point can be calculated to observe the energy distribution throughout the panel and how the severity of damage affects this. The WRMS is calculated at each scan point by using

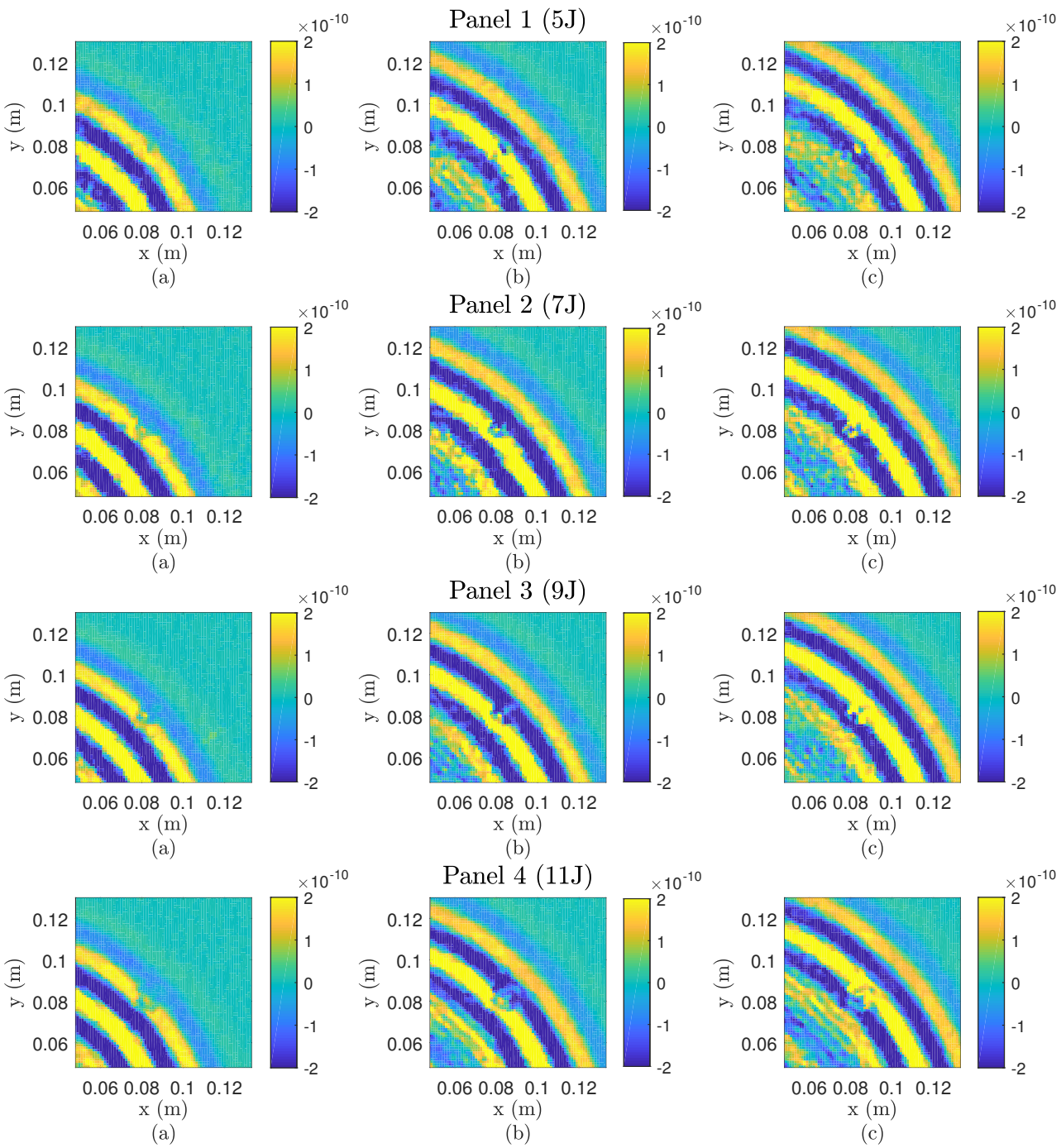

Figure 13. Impacted panels at 350kHz showing S_0 mode at (a) $34.4\mu s$, (b) $37.1\mu s$ and (c) $38.7\mu s$ respectively

$$u_{wrms}(x,y) = W(x,y)\sqrt{\frac{1}{N}\sum_{i=1}^{N} u(x,y,t)^2} \qquad (4)$$

where $u(x,y,t)$ is the displacement measured by the LDV and N is the number of discrete sampling points in time. Due to the attenuation of the waves, the RMS will obviously decrease with distance away from source. This means that high amplitudes at the points closest to the source do not necessarily indicate damage. In order to compensate for this, a weighting function, $W(x,y)$, was used which takes into account the distance of the scan point from the source, i.e. $W(x,y) = \sqrt{x^2+y^2}$, providing the source is at $(0,0)$. It is important to note that this only takes into account the effect of geometric spreading on the signals and not the material damping which is a function of frequency and wave mode as well the distance from the source. This WRMS was calculated for the same frequencies as the full wavefield signals in order to see the effects of both modes isolated as well as combined.

Figure 14 shows the WRMS distribution at 75kHz. In regards to severity, one can see that there is an increase in the WRMS amplitude at the damage location as the severity

increases. This could be down to trapped waves and mode conversions taking place in the damage zone. Then, beyond the damage, the WRMS creates a tapering shape of lower amplitude and the angle of this taper seems to be a function of the severity.

Figure 15 shows the WRMS distribution at 350kHz which should be mainly due to the S_0 mode at this frequency. Interestingly, unlike the A_0 mode (75kHz), there is no tapering effect or patterns of reflections around the damage area but just simply the area of damage given by points of a higher WRMS.

Wavenumber Filtering

When a sparse network of transducers is used to detect damage, a common SHM method of locating damage is to subtract the measured Lamb wave signals from a previously acquired baseline set of measurements. The theory is that any changes in the signal must be caused by reflections from damage that were not previously there. This is very difficult to do with a LDV due to the aligning of the lasers and the scan grid on the structure. However, one method of removing the propagating wave is through wavenumber filtering [34].

The wavenumber filtering works by converting the multidimensional LDV measured UGWs from the spatial domain to the wavenumber domain using a 2D Fourier transform for each time step as shown in Figure 16 and given by

$$Z_t\left(kx, ky\right) = \mathcal{F}_{2D}\left\{z_t\left(x, y\right)\right\}, \tag{5}$$

where $z_t\left(x, y\right)$ is the measured wavefield displacement defined by coordinates x and y at time point t, $F_{2D}\left\{\right\}$ is the 2D discrete Fourier transform and $Z_t\left(kx, ky\right)$ is the wavefield image at time point t in wavenumber domain. The dominant wavenumber, which corresponds to the propagating Lamb wave mode can then be determined and a 2D FIR filter mask using the 2D window method is proposed. This constructs a bandpass filter that is between 0.5 and 1.5 times the dominant wavenumber and is used to filter the wavefield image in the wavenumber domain using

$$\hat{Z}_t\left(kx, ky\right) = W\left(kx, ky\right) Z_t\left(kx, ky\right). \tag{6}$$

where $W\left(kx, ky\right)$ is the 2D window function and $\hat{Z}_t\left(kx, ky\right)$ is the filtered wavefield image. After this filter is applied to the data, the 2D discrete inverse Fourier transform is used to get back to the spatial domain by

$$\hat{z}_t\left(x, y\right) = \mathcal{F}_{2D}{}^{-1}\left\{\hat{Z}_t\left(kx, ky\right)\right\}. \tag{7}$$

where $\hat{z}_t\left(x, y\right)$ is the filtered wavefield image in the time domain. An example of this method is shown in Figure 16 for panel 4 at 50kHz and t = 0.113ms where the isolated reflections from the damage source can be seen after filtering.

Figure 17 shows the unfiltered 75kHz wavefield data in the spatial domain at t = 0.113ms. Here we can see the propagating wave being much larger in amplitude than damage reflections and therefore masking some of the more interesting reflection patterns. Using the proposed algorithm on that wavefield data, Figure 18 is obtained and the BVID sights can be seen clearly with increasing severity as a source of reflected waves. Even at higher frequencies where the wavelength is smaller such as in Figure 19 and Figure 20 for a 150kHz toneburst response at t = 0.107ms, this method still works.

LDV Conclusion

From the vast wealth of information obtained with the LDV, it was possible to characterise the through thickness damage severity by various wavefield analysis methods and by utilising the A_0 wave mode in particular.

By simply looking at the full wavefield at various timesteps, it was possible to see that the A_0 and S_0 modes interacted very differently with the impact damage and that the A_0 mode showed greater amplitude changes, phase shifts and reflections across the whole wavefield which became more pronounced with increasing severity. The S_0 mode showed none of these trends but the general shape and size of the impact damage could be seen, especially in the more severe case.

Similar observations could be made by looking at the WRMS of the wavefield. The interaction of the impact damage with the A_0 mode seemed to affect the whole propagating wavefield, especially as it got more severe, whilst the S_0 mode gave better outline of the impact damage location but not much information on its severity.

The A_0 mode's sensitivity to BVID severity was also apparent after filtering the data in the wavenumber domain to enhance the reflected waves coming from the BVID sights, showing a clear increase in reflections with increasing severity.

Incorporation into in-service SHM

Introduction

The full wavefield data obtained using the LDV showed that the A_0 mode's interaction with BVID was representative of increasing through thickness severity. In this section, an investigation is carried out to verify whether this can be applicable to a sparse network of transducers for in-service SHM. This is done by analysing signals captured only with other surface mounted PZTs. To do this, a fifth identical panel with no impact damage was manufactured and a network of four piezoelectric transducers were bonded to each of the five panels with the dimensions shown in Figure 21 for panel 4. Figure 22 shows the time domain signal and its corresponding Hilbert transform for each of the 5 panels in the direct path of the damage. Its clear to see from these figures how the amplitudes of the larger A_0 mode drop from the pristine case to the most severe case in the direct path. Not only this but the signal's phase shifts as the severity of the damage increases too which is in keeping with the observed results from the LDV.

However, without a baseline signal obtained when the panels were said to have been in a pristine state, it can be difficult to analyse what effect the damage itself has on the guided waves especially in the indirect paths as the reflection amplitudes are normally much smaller than the main toneburst. To overcome this problem, the fifth panel with no damage was used as a baseline and then impacted twice in the same location to increase the severity of the damage. Lamb wave measurements were taken before and

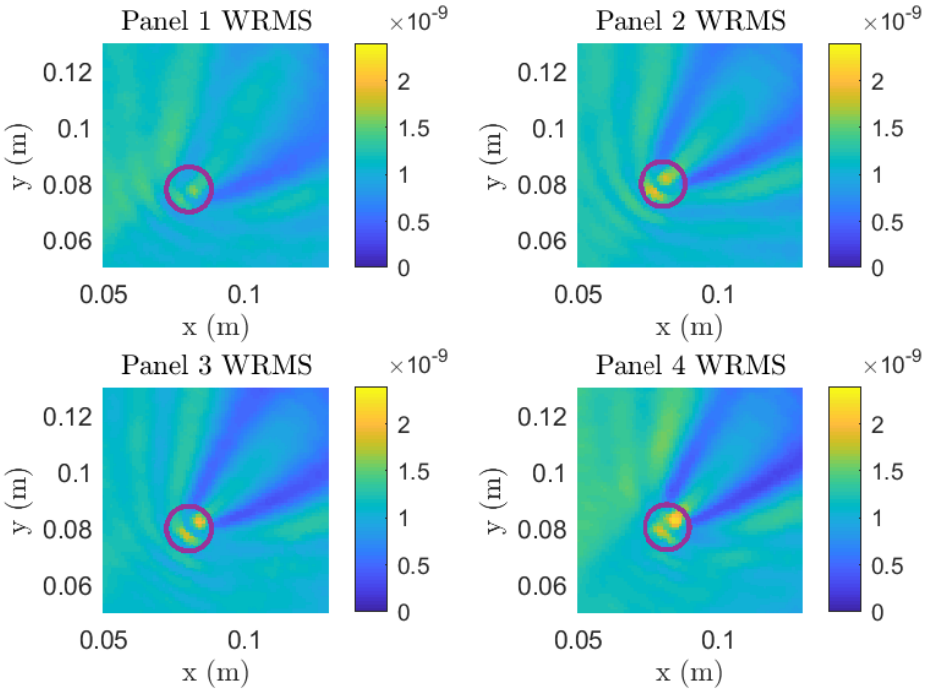

Figure 14. WRMS of the signals on the four panels at 75kHz with the impact location circled in purple

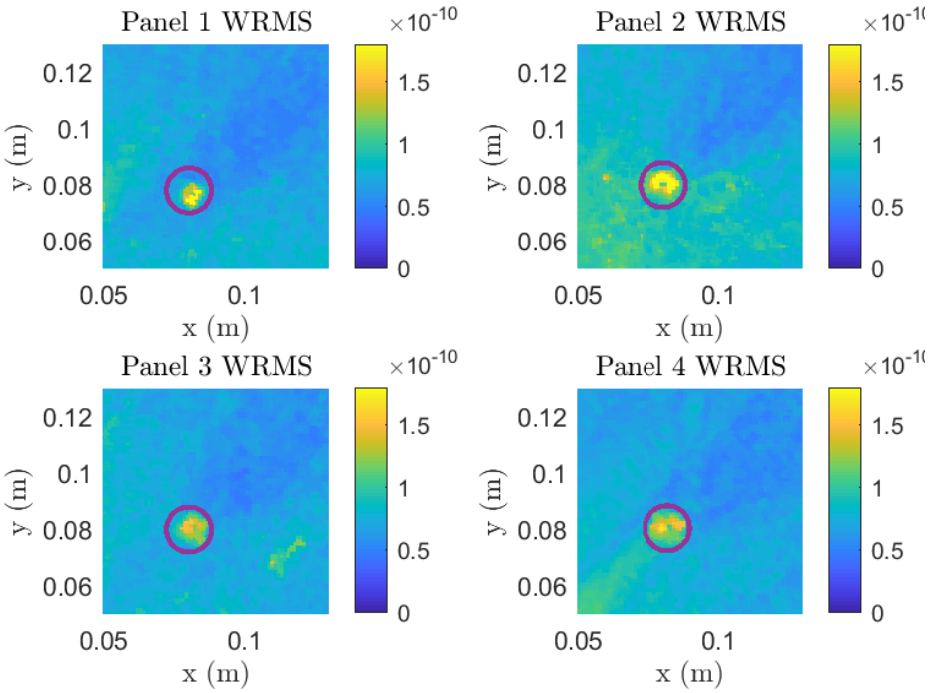

Figure 15. WRMS of the signals on the four panels at 350kHz with the impact location circled in purple

after each impact. In order to analyse more signal paths, another four PZT transducers were bonded to the pristine panel in the locations shown in Figure 23. The panel was then impacted with 5J first and then re-impacted with 7J in the same location. The Ultrasonic DolphiCam results after the 5J and 7J impact can be seen in Figure 24.

Delay & Sum Method

Many damage detection and localisation algorithms have been proposed for UGW based SHM. Often these are diagnostic imaging algorithms that give an intuitive and easy to understand image of the damage location. One popular imaging algorithm is the delay-and-sum technique [18, 19] which relies on the residual signals obtained by subtracting the current signals from a baseline signals corresponding to the pristine state. All of the residual signals are then shifted

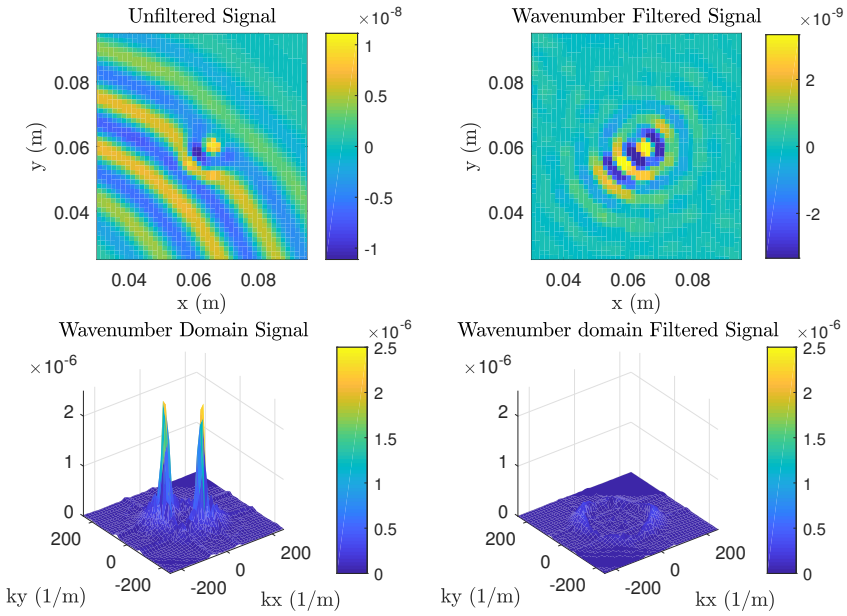

Figure 16. Wavefield data on panel 4 at t=0.113ms showing the principle of wavenumber filtering

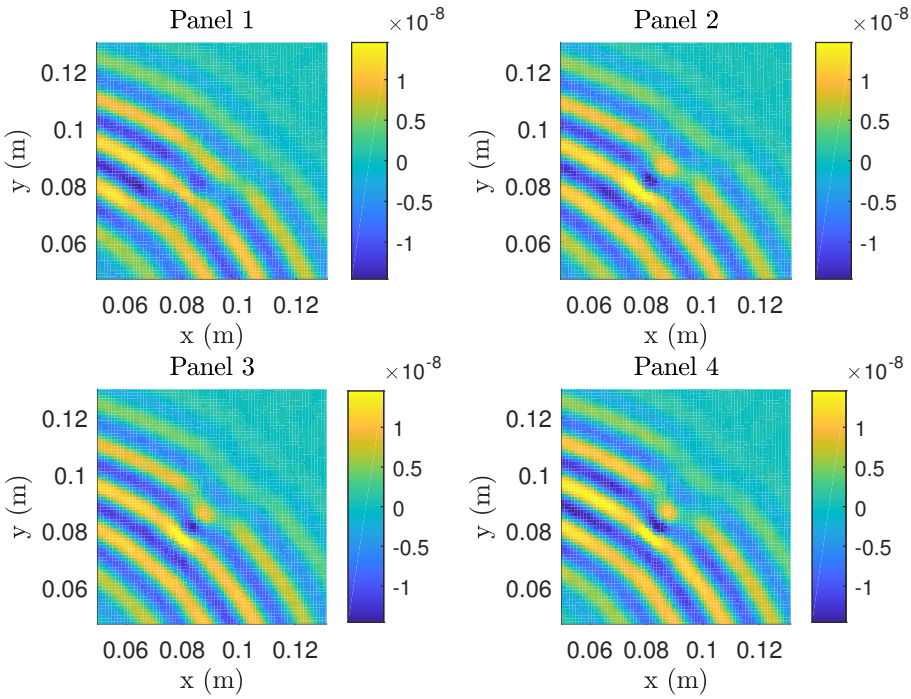

Figure 17. Wavefield data with a 75kHz toneburst on all four panels at t=0.113ms

according to an appropriate time shifting rule and summed to yield an average signal [4]. In this algorithm, the group velocity of the Lamb waves is of great importance to convert the time of arrival (ToA) of the wave packets to distance covered on the structure in order to localise the damage. This is one of the reasons that it's important to pick a suitable frequency that has low dispersion and one mode with much higher relative amplitudes to the others in order to assume a singular group velocity.

It was observed with the LDV that when the Lamb waves approach damage, they can get scattered by the localised change in material properties. So by using a baseline subtraction, the assumption is that the first wavepacket of the residual signal will be the scattered, damage reflected wave as demonstrated in Figure 25. If the group velocity known then it becomes possible to calculate the total distance from the actuator to the damage and then to the receiver. This can be used to construct an ellipse of possible damage locations where the actuator and sensor are the foci as can be seen in Figure 26 for path 4-8.

The basis of the delay & sum algorithm relies on a residual signal, $r_{as}(t)$, that is obtained by subtracting a

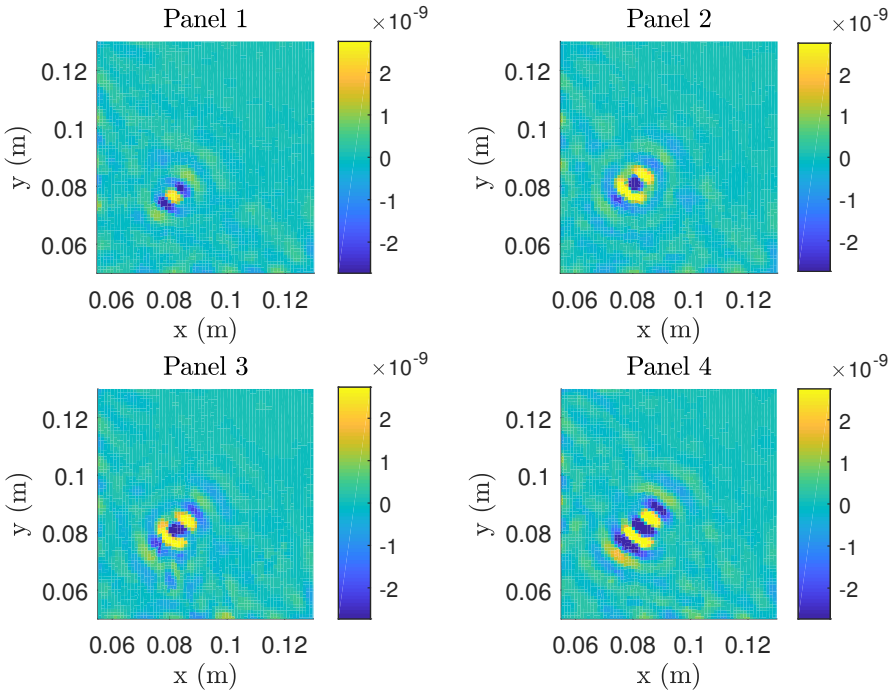

Figure 18. Wavefield data with a 75kHz toneburst on all four panels at t=0.113ms post wavenumber filtering showing the BVID severity

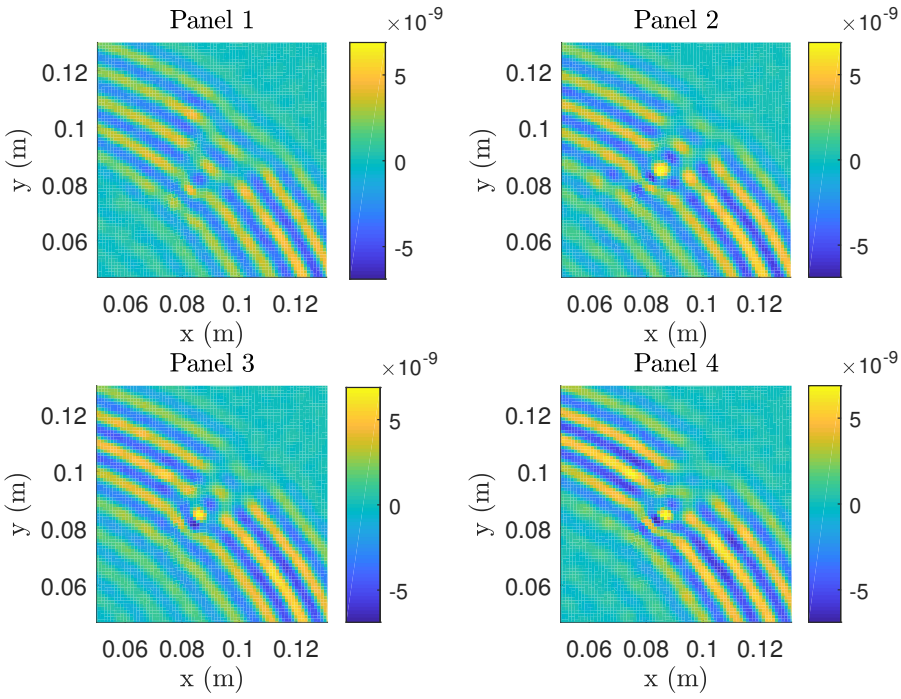

Figure 19. Wavefield data with a 150kHz toneburst on all four panels at t=0.107ms

previously acquired pristine baseline signal, $p_{as}(t)$, from the current signal, $c_{as}(t)$, for all N actuators and sensors $(a, s = 1, 2, ..., N)$. This is given by

$$r_{as}(t) = c_{as}(t) - p_{as}(t), \tag{8}$$

where the residual signal should only contain wave features that were not present when the structure was believed to be in a pristine state. To identify individual wavepackets, the envelope of the residual is determined by calculating the magnitude of the analytical signal given by

$$E_{as}(t) = \left| r_{as}(t) + j\mathcal{H}\left\{r_{as}(t)\right\}\right|, \tag{9}$$

where $\mathcal{H}$ is the Hilbert transform. As the damage location is unknown, the structure is discretised into pixels where each pixel is an image point (x, y) and the time of arrival

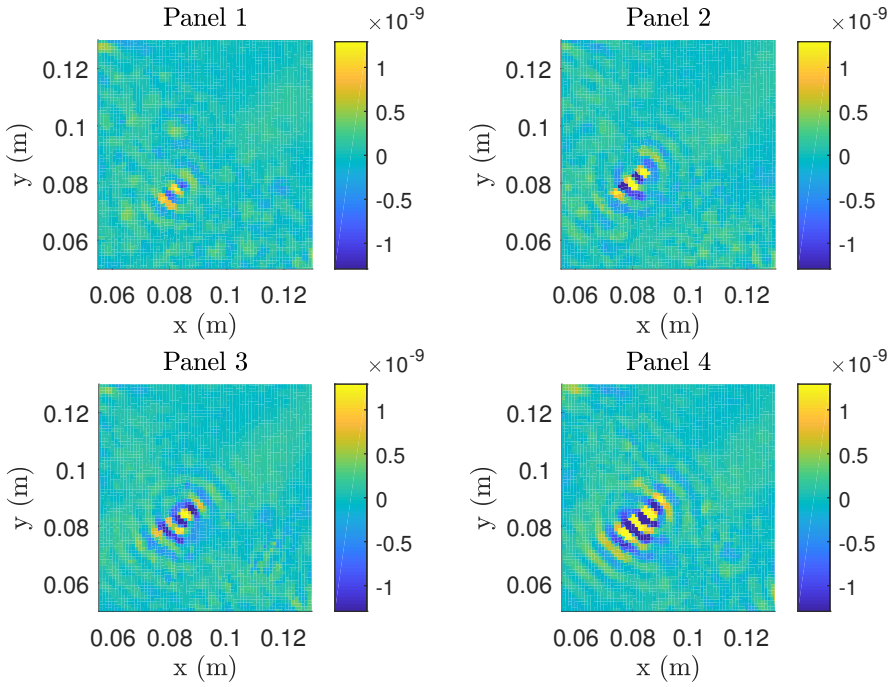

Figure 20. Wavefield data with a 150kHz toneburst on all four panels at t=0.107ms post wavenumber filtering showing the BVID severity

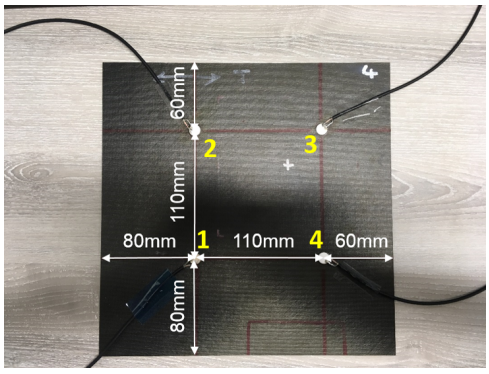

Figure 21. Dimensions of the transducer network bonded to each panel

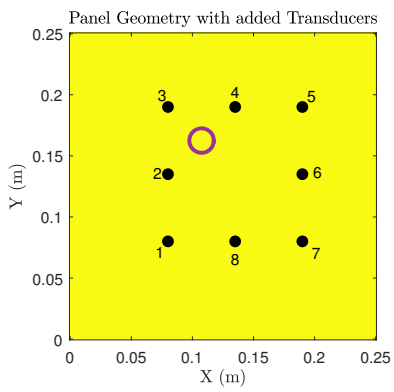

Figure 23. Transducer network numbering and impact location

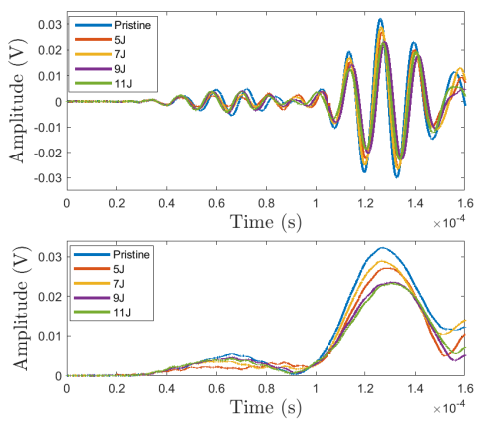

Figure 22. Time domain 75kHz signal response at path 1-3

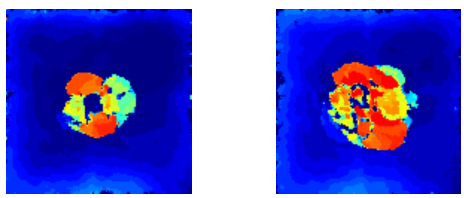

Figure 24. 5J (left) and 7J (right) impact C-scan

(ToA) for the wave to travel from the actuator to the pixel and then to the sensor, $t_{as}(x, y)$ is given by

$$t_{as}(x,y) = t_{off} + \frac{\sqrt{(x_a - x)^2 + (y_a - y)^2} + \sqrt{(x_s - x)^2 + (y_s - y)^2}}{c_g}, \tag{10}$$

where (x_a, y_a) and (x_s, y_s) are the actuator and sensor coordinates respectively, c_g, is the group velocity and t_{off} is a fixed offset corresponding to the time axis intercept

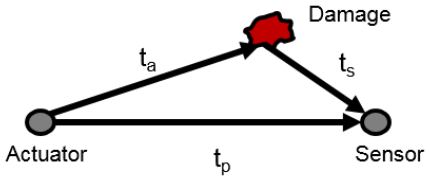

Figure 25. Baseline subtraction principle for one path showing the damage reflected ToA, $t_a + t_s$, compared to the pristine ToA, t_p

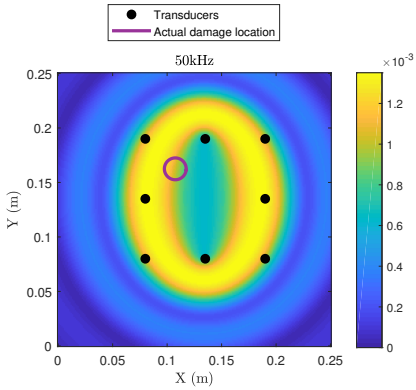

Figure 26. Ellipse formed from the residual of path 4-8 after 5J impact

when calculating the group velocity. The product of the residual signal with the discretised structure for a singular path then gives an image with an elliptical distribution of potential damage location as shown in Figure 26. Following the proposed delay-and-sum algorithm, the complete damage index, $DI(x, y)$, at each pixel for all possible paths is given by

$$DI\left(x,y\right) = \frac{1}{N}\sum_{a=1}^{N}\sum_{s=1,a\neq s}^{N} E_{as}\left(t_{as}\left(x,y\right)\right), \qquad (11)$$

where N is the number of paths, a is the actuator number and s is the sensor number. This damage detection algorithm was first used with the 5J impact and was then used again following the 7J impact. The required baseline was the same set of pristine signals measured before either impact.

Results

Individual paths near and far from the damage location for both 50kHz and 250kHz can be seen in Figures 27, 28, 29 and 30. It is clear from these figures that the A_0 mode is much more sensitive to damage severity. This is shown by the high amplitudes of the residuals in Path 2-4, with the more severe case having a much higher residual. Although the S_0 mode also shows higher residual amplitude in the more severe case in this path, the energies of both residuals are much less than those of the propagating waves themselves and are of similar magnitudes to the residuals in Path 6-8 which is far from the damage location. This validates the results obtained using the full wavefield information, which showed that the A_0 mode had higher sensitivity to damage severity.

Figure 31 shows the localisation of damage after the 5J impact whilst Figure 32 shows the localisation after the 7J impact, both at 50kHz. It is clear that the damage can be localised in both, with the most severe case having better localisation and a higher DI, which comes from the amplitudes of the residual, damage scattered signals. Again, this is in line with the observations obtained using the LDV.

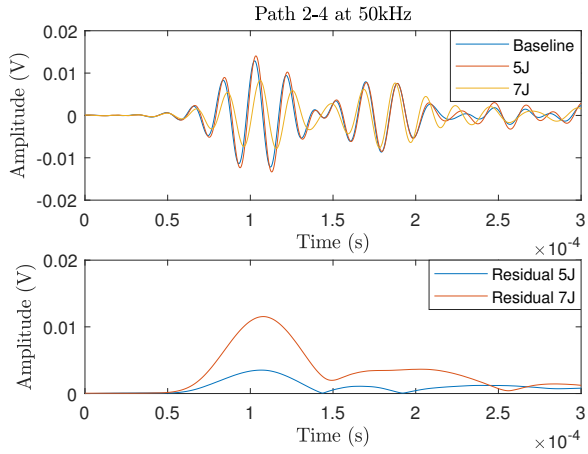

Figure 27. Signals on path 2-4 at 50kHz (left) and the corresponding residual signal envelope (right)

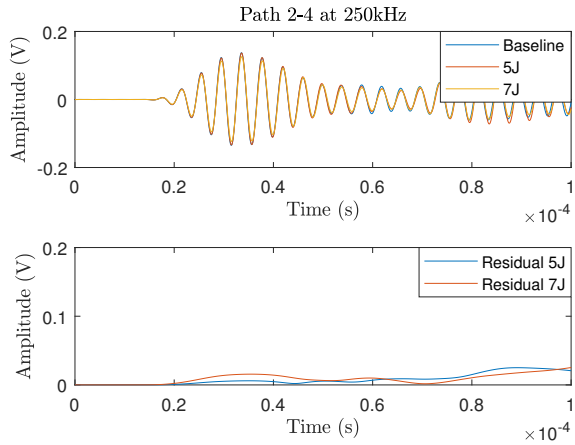

Figure 28. Signals on path 2-4 at 250kHz (left) and the corresponding residual signal envelope (right)

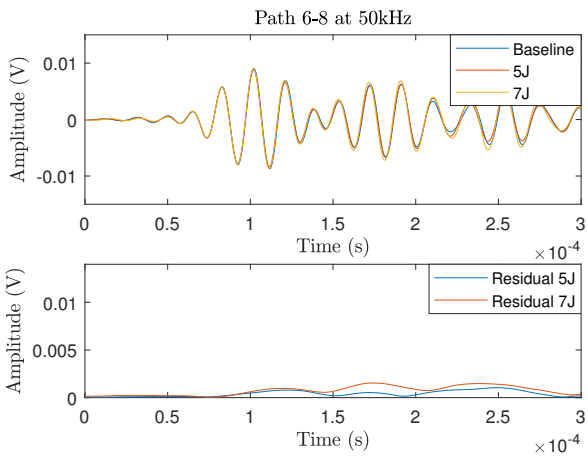

Figure 29. Signals on path 6-8 at 50kHz (left) and the corresponding residual signal envelope (right)

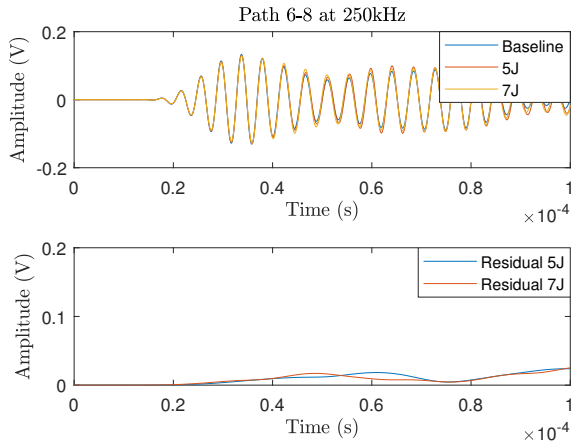

Figure 30. Signals on path 6-8 at 250kHz (left) and the corresponding residual signal envelope (right)

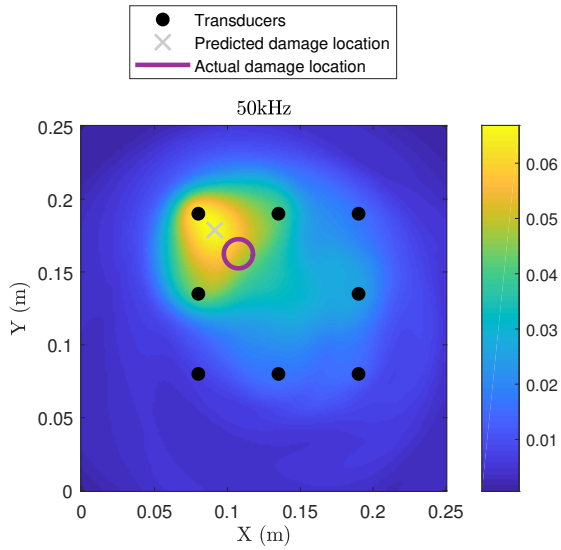

Figure 31. Damage localisation after the 5J impact at 50kHz

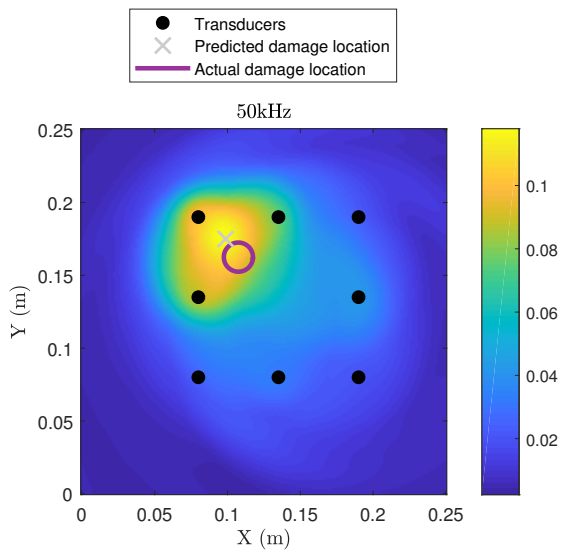

Figure 32. Damage localisation after the 7J impact at 50kHz

BVID Severity Damage Index

The localisation results showed that the more severe damage had a higher DI and a larger residual amplitude. Knowing the location of the damage from the delay & sum method, the severity of the BVID can then be analysed from the residual signals of individual paths near the predicted location of impact using a similar technique as that proposed by Sharif-Khodaei and Aliabadi for a multi-level decision fusion condition based maintenance based system [53]. By determining the envelope of the pristine signal, $P_{as}(t)$, for a path using

$$P_{as}(t) = \left|p_{as}(t) + j\mathcal{H}\left\{p_{as}(t)\right\}\right|, \tag{12}$$

and knowing its residual envelope, $(E_{as}(t))$, from the delay & sum method, which contains the damage reflected wavepackets. A severity DI is defined as

$$DI_s = \frac{max(E_{as}(t))}{max(P_{as}(t))}. \tag{13}$$

Figure 33 shows this DI_s for the actuator-sensor paths drawn from transducers 2, 3 & 4 near the predicted damage location whilst Figure 34 shows this DI_s for the actuator-sensor paths drawn from transducers 6, 7 & 8 far from the predicted damage location. It is clear to see from these results that the severity of damage can be analysed using paths near the predicted location of damage that was previously obtained with the delay & sum method. This demonstrates the potential of determining the severity of damage present in a structure using UGW based SHM.

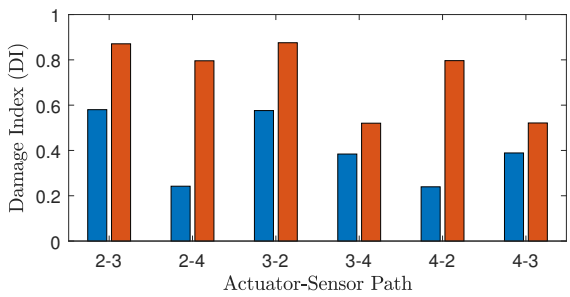

Figure 33. BVID severity DI after first impact (blue) and second impact (red) on paths near damage

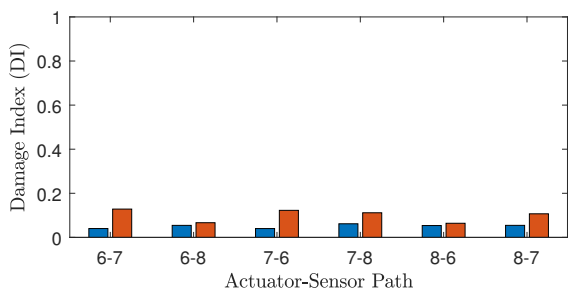

Figure 34. BVID severity DI after first impact (blue) and second impact (red) on paths far from damage

Conclusions

UGWs recorded with a LDV have been assessed to propose a measure of damage severity based on the scattering profile of the damage reflected wave for BVID present in composite plate-like structure. In particular, the two fundamental modes, A_0 and S_0, modes were compared and contrasted to see which frequency should be utilised in a SHM methodology for damage severity assessment. A chirp input signal and a post-processing toneburst reconstruction method was utilised to drastically reduce the acquisition time in determining the optimum input toneburst and to reduce the size of the data sets required. Four increasingly severe damage scenarios were looked at and the results showed that both modes could detect and localise the damage but the A_0 mode gave better severity assessment. This is due to the A_0 mode having greater through thickness sensitivity and higher attenuation.

As full wavefield analysis using the LDV is impractical as an in-service SHM technique, focus then turned to utilising UGWs with a sparse network of surface mounted transducers. BVID was first localised using a delay & sum imaging algorithm. The structure was impacted twice in the same location to increase the through thickness severity of damage and by looking at the residual signals of paths, it was clear that the A_0 mode was again more sensitive to the damage severity. After both impacts, the damage was localised and the more severe BVID had a higher localisation DI. Paths near the predicted damage location were then analysed individually and a severity DI_s was proposed using only the transducers near the impact location. All paths showed a higher DI_s with the more severe impact damage and a much higher DI_s than the paths far from damage.

Future work will contain further investigation into linking the damage severity index to the type of damage in the composite structure, e.g. debonding between skin/stiffener. The aim of this work was to characterise the severity of BVID, therefore different damage types were not investigated since the highest impact energy tested resulted in visible damage on the opposite face of the composite panel. In addition to this, machine learning algorithms could be trained and used to categorise the damage based on the reflected signals. More impact scenarios are required to be able to develop a reliable characterisation methodology. To save time and cost, numerical modelling is proposed to provide additional information alongside the experimental tests.

Acknowledgements

The authors would like to thank the UK Engineering and Physical Sciences Research Council (EPSRC) for funding this research.

References

[1] Giurgiutiu V. *Structural Health Monitoring with Piezoelectric Wafer Active Sensors*. Boston, MA: Academic Press, 2008.

[2] Rytter A. *Vibrational Based Inspection of Civil Engineering Structures*. PhD Thesis, Dept. of Building Technology and Structural Engineering, Aalborg University, Denmark, 1993.

[3] Staszewski W, Boller C and Tomlinson G. *Health Monitoring of Aerospace Structures*. Chichester: John Wiley & Sons, 2004.

[4] Michaels J and Michaels T. Guided wave signal processing and image fusion for in situ damage localization in plates. *Wave Motion* 2007; 44(6): 482 – 492. DOI:https://doi.org/10.1016/j.wavemoti.2007.02.008. URL http://www.sciencedirect.com/science/article/pii/S0165212507000212. Special Issue of Selected Papers Presented at the International Symposium on Mechanical Waves in Solids.

[5] Zhong C, Croxford A and Wilcox P. Remote inspection system for impact damage in large composite structure. *Proceedings of the Royal Society of London A: Mathematical, Physical and Engineering Sciences* 2015; 471(2173). DOI:10.1098/rspa.2014.0631. URL http://rspa.royalsocietypublishing.org/content/471/2173/20140631.

[6] Flynn E, Todd M, Wilcox P et al. Maximum-likelihood estimation of damage location in guided-wave structural health monitoring. *Proceedings of the Royal Society of London A: Mathematical, Physical and Engineering Sciences* 2011; DOI:10.1098/rspa.2011.0095.

[7] Hall J, McKeon P, Satyanarayan L et al. Minimum variance guided wave imaging in a quasi-isotropic composite plate. *Smart Materials and Structures* 2011; 20(2): 025013.

[8] Moll J, Torres-Arredondo M and Fritzen C. Computational aspects of guided wave based damage localization algorithms in flat anisotropic structures. *Smart Structures and Systems* 2012; 10: 229–251.

[9] Kijanka P, Manohar A, Lanza di Scalea F et al. Damage location by ultrasonic lamb waves and piezoelectric rosettes. *Journal of Intelligent Material Systems and Structures* 2014; 26: 1477–1490.

[10] Jarmer G, Flynn E and Todd M. Multi-wave-mode, multi-frequency detectors for guided wave interrogation of plate structures. *Structural Health Monitoring* 2013; 13: 120–130.

[11] He J and Yuan F. Damage identification for composite structures using a cross-correlation reverse-time migration technique. *Structural Health Monitoring* 2015; 14(6): 558–570. DOI:10.1177/1475921715602546.

[12] Mitra M and Gopalakrishnan S. Guided wave based structural health monitoring: A review. *Smart Materials and Structures* 2016; 25(5): 053001.

[13] Su Z and Ye L. *Identification of Damage Using Lamb Waves: From Fundamentals to Applications*. Lecture Notes in Applied and Computational Mechanics, Springer London, 2009.

[14] Torkamani S, Roy S, Barkey M et al. A novel damage index for damage identification using guided

waves with application in laminated composites. *Smart Materials and Structures* 2014; 23(9): 095015.

[15] Huang L, Zeng L, Lin J et al. An improved time reversal method for diagnostics of composite plates using lamb waves. *Composite Structures* 2018; 190: 10–19.

[16] Zhao X, Gao H, Zhang G et al. Active health monitoring of an aircraft wing with embedded piezoelectric sensor/actuator network: I. defect detection, localization and growth monitoring. *Smart Materials and Structures* 2007; 16(4): 1208. URL http://stacks.iop.org/0964-1726/16/i=4/a=032.

[17] Liu Z, Zhong X, Dong T et al. Delamination detection in composite plates by synthesizing time-reversed lamb waves and a modified damage imaging algorithm based on rapid. *Structural Control and Health Monitoring* 2017; 24(5): e1919.

[18] Michaels J. Detection, localization and characterization of damage in plates with an in situ array of spatially distributed ultrasonic sensors. *Smart Materials and Structures* 2008; 17(3): 035035. URL http://stacks.iop.org/0964-1726/17/i=3/a=035035.

[19] Sharif-Khodaei Z and Aliabadi M. Assessment of delay-and-sum algorithms for damage detection in aluminium and composite plates. *Smart Materials and Structures* 2014; 23(7): 075007. URL http://stacks.iop.org/0964-1726/23/i=7/a=075007.

[20] Salmanpour M, Sharif Khodaei Z and Aliabadi M. Guided wave temperature correction methods in structural health monitoring. *Journal of Intelligent Material Systems and Structures* 2017; 28(5): 604–618.

[21] Lu G, Li Y, Wang T et al. A multi-delay-and-sum imaging algorithm for damage detection using piezoceramic transducers. *Journal of Intelligent Material Systems and Structures* 2017; 28(9): 1150–1159.

[22] Zeng L, Huang L and Lin J. Damage imaging of composite structures using multipath scattering lamb waves. *Composite Structures* 2019; .

[23] Ihn J and Chang F. Detection and monitoring of hidden fatigue crack growth using a built-in piezoelectric sensor/actuator network: I. diagnostics. *Smart materials and structures* 2004; 13(3): 609.

[24] Ihn J and Chang F. Detection and monitoring of hidden fatigue crack growth using a built-in piezoelectric sensor/actuator network: Ii. validation using riveted joints and repair patches. *Smart materials and structures* 2004; 13(3): 621.

[25] Memmolo V, Monaco E, Boffa N et al. Guided wave propagation and scattering for structural health monitoring of stiffened composites. *Composite Structures* 2018; 184: 568–580.

[26] Pillarisetti L and Talreja R. On quantifying damage severity in composite materials by an ultrasonic method. *Composite Structures* 2019; 216: 213–221.

[27] Staszewski W, Lee B, Mallet L et al. Structural health monitoring using scanning laser vibrometry: I. lamb wave sensing. *Smart Materials and Structures* 2004; 13(2): 251.

[28] Mallet L, Lee BC, Staszewski wJ et al. Structural health monitoring using scanning laser vibrometry: Ii. lamb waves for damage detection. *Smart Materials and Structures* 2004; 13(2): 261. URL http://stacks.iop.org/0964-1726/13/i=2/a=003.

[29] Leong W, Staszewski W, Lee B et al. Structural health monitoring using scanning laser vibrometry: Iii. lamb waves for fatigue crack detection. *Smart Materials and Structures* 2005; 14(6): 1387.

[30] Staszewski W, bin Jenal R, Klepka A et al. A review of laser doppler vibrometry for structural health monitoring applications. In *Structural Health Monitoring II*, *Key Engineering Materials*, volume 518. Trans Tech Publications, pp. 1–15. DOI:10.4028/www.scientific.net/KEM.518.1.

[31] Ruzzene M, Jeong S, Michaels T et al. Simulation and measurement of ultrasonic waves in elastic plates using laser vibrometry. *AIP Conference Proceedings* 2005; 760(1): 172–179. DOI:10.1063/1.1916675.

[32] Kudela P, Radzieski M and Ostachowicz W. Identification of cracks in thin-walled structures by means of wavenumber filtering. *Mechanical Systems and Signal Processing* 2015; 50-51: 456 – 466. DOI:https://doi.org/10.1016/j.ymssp.2014.05.041.

[33] Zak A, Radzienski M, Krawczuk M et al. Damage detection strategies based on propagation of guided elastic waves. *Smart Materials and Structures* 2012; 21(3): 035024. URL http://stacks.iop.org/0964-1726/21/i=3/a=035024.

[34] Ruzzene M. Frequencywavenumber domain filtering for improved damage visualization. *Smart Materials and Structures* 2007; 16(6): 2116. URL http://stacks.iop.org/0964-1726/16/i=6/a=014.

[35] Rogge MD and Leckey CA. Characterization of impact damage in composite laminates using guided wavefield imaging and local wavenumber domain analysis. *Ultrasonics* 2013; 53(7): 1217 – 1226. DOI: https://doi.org/10.1016/j.ultras.2012.12.015.

[36] Chia C, Lee J, Park C et al. Laser ultrasonic anomalous wave propagation imaging method with adjacent wave subtraction: Application to actual damages in composite wing. *Optics & Laser Technology* 2012; 44(2): 428 – 440. DOI:https://doi.org/10.1016/j.optlastec.2011.08.007.

[37] Pieczonka Ł, Ambroziński Ł, Staszewski W et al. Damage detection in composite panels based on mode-converted lamb waves sensed using 3d laser scanning vibrometer. *Optics and lasers in engineering* 2017; 99: 80–87.

[38] Park B, An Y and Sohn H. Visualization of hidden delamination and debonding in composites through noncontact laser ultrasonic scanning. *Composites Science and Technology* 2014; 100: 10 – 18. DOI:https://doi.org/10.1016/j.compscitech.2014.05.029. URL http://www.sciencedirect.com/science/article/pii/S0266353814001845.

[39] Yu L, Tian Z and Leckey C. Crack imaging and quantification in aluminum plates with guided wave wavenumber analysis methods. *Ultrasonics* 2015; 62: 203–212.

[40] Tian Z, Yu L and Leckey C. Rapid guided wave delamination detection and quantification in composites using global-local sensing. *Smart Materials and Structures* 2016; 25(8): 085042.

[41] Mesnil O and Ruzzene M. Sparse wavefield reconstruction and source detection using compressed sensing. *Ultrasonics* 2016; 67: 94–104.

[42] Dafydd I and Sharif Khodaei Z. Laser vibrometer imaging of delamination interaction with lamb waves using a chirp excitation method. In *Advances in Fracture and Damage Mechanics XVI*, *Key Engineering Materials*, volume 754. Trans Tech Publications, pp. 375–378.

[43] Dafydd I and Sharif Khodaei Z. Damage severity assessment in composite structures using ultrasonic guided waves with chirp excitation. *ProcSPIE* 2018; 10598: 10598 – 10598 – 11. DOI:10.1117/12.2299647. URL https://doi.org/10.1117/12.2299647.

[44] Hall J and Michaels J. Multipath ultrasonic guided wave imaging in complex structures. *Structural Health Monitoring* 2015; 14(4): 345–358.

[45] Olsson R. Analytical prediction of large mass impact damage in composite laminates. *Composites Part A: Applied Science and Manufacturing* 2001; 32(9): 1207 – 1215. DOI:https://doi.org/10.1016/S1359-835X(01)00073-2.

[46] Bossi R and Giurgiutiu V. Nondestructive testing of damage in aerospace composites. In Irving P and Soutis C (eds.) *Polymer Composites in the Aerospace Industry*. Woodhead Publishing. ISBN 978-0-85709-523-7, 2015. pp. 413 – 448. DOI:https://doi.org/10.1016/B978-0-85709-523-7.00015-3. URL http://www.sciencedirect.com/science/article/pii/B9780857095237000153.

[47] Ciampa F, Mahmoodi P, Pinto F et al. Recent advances in active infrared thermography for non-destructive testing of aerospace components. *Sensors* 2018; 18(2). DOI:10.3390/s18020609. URL http://www.mdpi.com/1424-8220/18/2/609.

[48] Michaels J. Ultrasonic wavefield imaging: Research tool or emerging nde method? *AIP Conference Proceedings* 2017; 1806(1): 020001. DOI:10.1063/1.4974542. URL https://aip.scitation.org/doi/abs/10.1063/1.4974542.

[49] Waldbronn PG. *PSV-500-3D Scanning Vibrometer*. 2016.

[50] Wilcox PD, Dalton RP, Lowe MJS et al. Mode and transducer selection for long range lamb wave inspection. In *Key Engineering Materials*, volume 167. Trans Tech Publications, pp. 152–161.

[51] Michaels JE, Lee SJ, Croxford AJ et al. Chirp excitation of ultrasonic guided waves. *Ultrasonics* 2013; 53(1): 265 – 270. DOI:https://doi.org/10.1016/j.ultras.2012.06.010.

[52] Michaels JE, Lee SJ, Hall Js et al. Multi-mode and multi-frequency guided wave imaging via chirp excitations. *ProcSPIE* 2011; 7984: 7984 – 7984 – 11. DOI:10.1117/12.880963. URL http://dx.doi.org/10.1117/12.880963.

[53] Sharif Khodaei Z and Aliabadi M. A multi-level decision fusion strategy for condition based maintenance of composite structures. *Materials* 2016; 9(9): 790.